DALTON
FULL PAPER

The Mayer bond order as a tool in inorganic chemistry †

Adam J. Bridgeman,*[a] Germán Cavigliasso,[b] Luke R. Ireland[a] and Joanne Rothery[b]

[a] *Department of Chemistry, University of Hull, Kingston-upon-Hull, UK HU6 7RX. E-mail: a.j.bridgeman@chem.hull.ac.uk*
[b] *Department of Chemistry, University of Cambridge, Lensfield Road, Cambridge, UK CB2 1EW*

Received 6th March 2001, Accepted 31st May 2001
First published as an Advance Article on the web 3rd July 2001

The bonding in molecules is most often described using the classical chemical ideas of covalency (bond multiplicity) and ionicity (atomic charges). The Mayer bond order is a natural extension of the Wiberg bond order, which has proved extremely useful in bonding analysis using semi-empirical computational methods, and the Mulliken population analysis to *ab initio* theories. The usefulness of the Mayer bond order has been tested in a number of inorganic molecules including sulfur–nitrogen rings, halogen–oxide molecules and transition metal dichloride molecules. The basis set dependence of the Mayer bond order is tested through the case studies presented. It is shown that the bond order can be fully or partially decomposed into the contributions from symmetry types for many interactions of interest to the inorganic chemist. The power of this approach is shown by examining the bonding in a variety of systems and is illustrated by detailed studies of the role of the ring size and electron count on the bonding in S–N rings, the role of hypervalency in the relative stabilities of mixed hydrogen and halogen peroxide isomers and the importance of s–d hybridization in the 3d transition metal dichloride molecules.

The ideas of bond order, index and valence are key to our everyday understanding of chemistry and chemical processes. They are implicit in every chemical structure that is drawn and are central to the teaching of inorganic chemistry at all levels. Whilst quantum theory and modern ideas of electronic structure provide a quantitative rationalization of chemical bonding and structure, useful chemical notions such as atomic charge, valence and bond order for which no quantum mechanical operator can be deduced lose focus and status.

A number of methods or prescriptions for the calculation of bond order from molecular orbital calculations have been proposed. Probably the simplest is that proposed by Coulson[1] for π-orbitals at the Hückel level. In this definition, the bond order between atoms A and B is given by,

$$B_{\mathbf{AB}} = \sum_i c_{i\mathbf{A}} c_{i\mathbf{B}} \tag{1}$$

where $c_{i\mathbf{A}}$ is the coefficient of the atomic orbital $\varphi_{\mathbf{A}}$ on atom A in the i^{th} doubly occupied molecular orbital θ_i,

$$\theta_i = \sum_i c_{i\mathbf{A}} \varphi_{\mathbf{A}} \tag{2}$$

and normalization is implicit in the definition of the coefficients. The Coulson bond orders in a molecule, given by eqn. (1), are the off-diagonal terms of the matrix **P** whose elements are given in general as,

$$\mathrm{P}_{st} = \sum_i^{\text{occupied}} n_i c_{rs} c_{rt} \tag{3}$$

where the summation is over the molecular orbitals with occupation numbers n_i. **P** is known as the density matrix as the electron density ρ is,

$$\rho = \sum_s \sum_t \mathrm{P}_{st} \varphi_s \varphi_t \tag{4}$$

In a zero-overlap model such as Hückel theory, the diagonal elements are the atomic charges and the total number of electrons in the molecule is given by their sum. **P** is often also referred to as the bond-order matrix. In calculations beyond the simple minimal basis Hückel approach, the summation in eqn. (2) for the molecular orbital involves a number of orbitals on each atomic centre. The bond order definition given in eqn. (1) must be generalized by summing over each of the off-diagonal terms in **P** involving the orbitals of each atom,

$$B_{\mathbf{AB}} = \sum_s^{\text{on A}} \sum_t^{\text{on B}} \mathrm{P}_{st} \tag{5}$$

An alternative definition of bond order due to Wiberg[2] is also based on the **P** matrix and is applicable to NDO-type theories where the atomic orbital basis forms an orthonormal set. The Wiberg bond order uses the *square* of the off-diagonal elements of **P**,

$$B_{\mathbf{AB}}^{\text{Wiberg}} = \sum_s^{\text{on A}} \sum_t^{\text{on B}} \mathrm{P}_{st}^2 \tag{6}$$

This definition leads to intrinsically positive bond orders between all atoms in a molecule. Wiberg bond orders are closer to classical bond valences and are implemented in many semi-empirical electronic structure codes. In *ab initio* molecular orbital theories, a basis set of non-orthogonal atomic orbitals is generally used and overlap is included. The total number of electrons in a molecule is given by integrating eqn. (4) over all space,

$$N = \sum_s \mathrm{P}_{ss} + \sum_s \sum_{t \neq s} \mathrm{P}_{st} \mathrm{S}_{st} \tag{7}$$

where **S** is the atomic orbital overlap matrix. The off-diagonal matrix elements of **PS** are known as Mulliken overlap populations and are, by analogy with the Coulson definition, often taken as a measure of the contribution from each pair of

† Electronic supplementary information (ESI) available: calculated structures of $X'XO_2$, X′OXO, XO_2, X′OX, X′XO and XO. See http://www.rsc.org/suppdata/dt/b1/b102094n/

orbitals to the strength of the chemical bonds. Mayer[3] has suggested a method for calculating bond orders from the **P** matrix,

$$B_{AB}^{Mayer} = \sum_{s}^{\text{on A}} \sum_{t}^{\text{on B}} (\mathbf{PS})_{st}(\mathbf{PS})_{ts} \quad (8)$$

The Mayer definition can be seen as an extension of the Wiberg index. This leads to the classical integer values for homonuclear diatomics when minimal or small basis sets are used. Non-integer values are found for larger basis sets and in more complicated molecules and these reflect the ionic character of the bonds as well as delocalization and multicentre effects. We have found it is an invaluable tool in the analysis of the bonding in main group[4] and transition metal[5] systems. The insight that can be obtained into the strength and nature of the bonding using the Mayer bond order is demonstrated by a number of case studies in this paper, drawn from a variety of areas of the periodic table.

The relationship of the Mayer bond order to the Mulliken population is clear from the definitions given above. The basis set dependence of the Mulliken population analysis is well known, although Mayer[3] has also shown that its form is fully consistent with the molecular orbital approach rather than an arbitrary choice. The basis set dependence of the Mayer bond order has been less thoroughly studied. In this paper, this has been investigated both for some simple, electron precise molecules and for systems where classical ideas of valency are less applicable. The calculations presented use density functional theory to obtain the density matrix. The dependence of the Mulliken charges and bond orders on the exchange and correlation functionals is also studied using a variety of local, non-local and hybrid functionals.

The expectation of the chemist is that the order of a bond is related to the strength and hence to the length of the bond. Pauling and co-workers[6] suggested a simple function to reflect the expected correlation between bond order and length,

$$B_{AB} = \exp\left(\frac{-(r - r_0)}{b}\right) \quad (9)$$

which suggests that the bond order increases or decreases exponentially as the bond length, r, decreases or increases with respect to the length of the single bond, r_0. The latter may or may not be known so that r_0 as well as the parameter b are fitted empirically. This requires knowledge of the order of a bond at a number of different lengths. The Pauling correlation is extensively used in the bond valence model. In this approach, the bond valences about an atom sum up to give the absolute amount of the atom's oxidation state. By assigning classical values to the bonds in the simplest systems, the bond valences in more complicated molecules are determined by fitting to the Pauling or related formula.

Lendvay[7] has studied the predictions of the Mayer definition for C–C, C–O and C–H bonds and found that the Pauling formula describes the correlation extremely well. In this paper, the bond length/bond order correlation is further investigated for a number of bonds characterized by strong bond length variations. It may be noted that the dependence of the Mayer bond order on bond length does *not* arise from the inclusion of orbital overlap in its definition. When a non-orthogonal basis set is used, the normalization of the molecular orbital leads to orbital coefficients that are dependent on the atomic orbital overlaps. The calculation of the Coulson or Wiberg bond orders using the molecular orbitals generated using such a basis set then introduces this overlap dependence. The multiplication of the **P** and **S** matrices removes this dependence in the Mayer definition, as may be simply demonstrated for a molecule such as H_2. The variation in the order of the bond between atoms A and B with its length in a set of molecules containing a variety of substituents on the two atoms thus reflects the redistribution of electron density and the differing electronic demands of the molecular fragments.

Orbital symmetry plays a central role in bonding theory based on the concepts of molecular orbital models. As well as aiding the computational efficiency of electronic structure codes, it has a strong influence on the teaching and description of covalent bonding. Thus, bonding interactions are often separated into σ, π and δ-interactions even in molecules where these labels are inappropriate. The synergistic roles of σ-donation and π-acceptance by ligands such as CO and olefins in organometallic compounds of many different shapes is used, for example, as a powerful tool for the understanding and prediction of molecular properties. Symmetry allows the chemist to build up the complex electron density in a molecule and decompose the bonding into the orbital contributions from fragments.

The definition of the **P** matrix, given in eqn. (3), may be rewritten by grouping together the occupied orbitals into symmetry types Γ,

$$\mathbf{P} = \sum_{\Gamma}^{\text{sym types}} \mathbf{P}^{\Gamma} \quad (10)$$

Similarly, the **PS** matrix may be rewritten as a sum over symmetry types,

$$\mathbf{PS} = (\sum_{\Gamma} \mathbf{P}^{\Gamma})\mathbf{S} = \sum_{\Gamma} (\mathbf{PS})^{\Gamma} \quad (11)$$

The Mayer bond order given in eqn. (8) then becomes,

$$B_{AB}^{Mayer} = \sum_{r}^{\text{on A}} \sum_{t}^{\text{on B}} (\sum_{\Gamma_i} \mathbf{PS}_{st}^{\Gamma_i})(\sum_{\Gamma_j} \mathbf{PS}_{ts}^{\Gamma_j}) \quad (12)$$

As long as the orbitals s and t, centred on atoms A and B respectively, only occur in *one* common symmetry species at most, there are no cross-terms arising from the two summations in brackets in eqn. (12). In this case, the bond order is given as a sum over symmetry species,

$$B_{AB}^{Mayer} = \sum_{\Gamma} B_{AB}^{\Gamma} \quad (13)$$

This is the case in very many complexes for the bonds to the central element. In these systems, the atomic orbitals of the central element each span a single symmetry species. Each atomic orbital on the central atom only occurs in molecular orbitals with ligand orbitals of one symmetry type. 'Cross terms' in eqn. (12) of the type $(\mathbf{P}^{\Gamma i}\mathbf{S})_{st}$ $(\mathbf{P}^{\Gamma j}\mathbf{S})_{ts}$ are zero unless $i = j$. The Mayer bond order can then be broken down into its contributions from orbitals of each symmetry type. A number of examples showing the effectiveness of this decomposition are discussed in this paper.

Eqn. (13) does not apply when s and t occur in more than one symmetry species. This may be the case in high symmetry molecules if there is more than one atom of type A *and* of type B. The two atoms in a homonuclear diatomic, for example, are equivalent by symmetry. Each orbital on atom A occurs in molecular orbitals of two symmetry types labelled as g and u. The equivalent orbital on atom B occurs in the same two symmetry types. The cross terms in eqn. (12) are non-zero. It is similarly not possible to compute the contributions by symmetry type to the C–H or C–C bond orders in the benzene molecule as there are six equivalent C and six equivalent H atoms.

Even in these cases, some information about the contributions can still be obtained by summing over sets of symmetry types. In the homonuclear diatomic, there are no atomic orbitals which occur in both σ and π molecular orbitals. No cross terms therefore occur in the summation if the $\mathbf{PS}^{\Gamma}$

matrices are added together for the g and u parts of the σ, π, δ, . . . orbitals. Similarly, in the benzene ring, there is a complete separation of the atomic orbitals into those symmetric and asymmetric with respect to the σ_h plane and thus the in-plane and out-of-plane contributions to the C–C bonding can be obtained. The most useful separation into σ and π bond orders is thus possible.

In molecules with low symmetry, there is often only one symmetry equivalent atom of each type and this problem is not relevant. In such molecules, however, the small number of symmetry species reduces the relevence of symmetry in understanding the bonding and the usefulness of the decomposition.

Computational details

All of the calculations used density functional methods to calculate eigenvectors and to optimize geometries where appropriate. Calculations were performed using four computational packages: Gaussian98,[8] Gamess-UK version 6.2,[9] ADF version 2000.02[10] and DeFT.[11] A variety of different levels of theory were used to investigate the effects on the calculated bond orders. The Vosko, Wilk and Nusair correlation functional[12] was used for local density approximation (LDA) calculations. Non-local calculations were performed with Becke's 1988 exchange functional[13] in combination with Perdew's 1986 correlation functional[14] (BP86) and with the correlation functional of Lee, Yang and Parr[15] (BLYP). Calculations have also been performed using two of the most popular hybrid functionals which mix Hartree–Fock exchange with the non-local exchange-correlation functional listed above (B3LYP and B3P86).[16] A variety of different basis sets have been employed of Slater and Gaussian type orbitals (STOs and GTOs respectively) with varying numbers of functions and contraction patterns. GTOs are employed in the Gaussian98, Gamess-UK and DeFT codes. STOs are used in ADF. These are given in each of the subject areas below with their standard shorthand labels. Natural bond orbital (NBO) populations were calculated using the NBO routines[17] in Gaussian98. Atomic charges and bond orders were also calculated using Bader's atoms in molecules (AIM) approach[18] as implemented[19] in Gaussian98.

The calculation of the Mayer bond order requires the density and overlap matrices. Only the Gamess-UK code of the four programs used has the option of calculating Mayer bond orders. Even in this case, there is not the facility to partition the bond orders using symmetry, as outlined above. A program has therefore been written to read in the eigenvectors and, where possible, the overlap matrix from the output of the programs and subsequently to calculate the Mayer bond orders. The program MAYER[20] is available on request from the authors.

Results and discussion

(a) Classical main group molecules

Mayer has reported[3] bond order calculations on a number of simple main group molecules such as homonuclear diatomics, water and small organic molecules with minimal and small double-ζ basis sets (STO-3G and 4-31G respectively). The minimal basis set calculations were found to give bond orders close to classical valence values. The larger basis set led to somewhat reduced bond orders. Tables 1 and 2 list bond orders calculated for a number of diatomic and triatomic molecules using Gamess-UK and ADF respectively with a variety of functionals and basis sets. Tables 3 and 4 list analogous bond orders for some polyatomic molecules. The molecules chosen include some of those selected by Mayer and more complex systems such as diborane, N_2O and the adduct NH_3–BH_3 where the bonding is less easily described using classical valence ideas. For each molecule, the calculations were performed on the same, standard geometry to remove any dependence of the bond order on the detailed geometry. The bond orders are only listed for the pairs of atoms which are conventially connected in each molecule. The bond orders for the other atom pairs are found to be close to, but not necessarily equal to, zero. These low numbers result from equal populations of molecular orbitals which are bonding and antibonding with respect to the atoms. In a molecule like diborane where multicentre bonding is

Table 1 Mayer bond orders for a set of simple di- and triatomic main group molecules calculated using Gamess-UK

Method Basis set		LDA cc-pvdz	BP86 cc-pvdz	B3LYP cc-pvdz	B3LYP tzvp	B3LYP cc-pvtz
H_2		1.00	1.00	1.00	1.00	1.00
CO		2.66	2.64	2.62	2.38	2.52
CO_2		2.27	2.25	2.25	2.09	2.25
N_2		2.87	2.84	2.87	2.89	2.93
N_2O	N–N	2.31	2.27	2.32	2.34	2.38
	N–O	1.75	1.71	1.70	1.63	1.83
F_2		0.99	0.99	0.98	0.94	0.97
HF		1.05	1.06	1.05	0.91	1.04
H_2O		1.03	1.04	1.03	0.93	1.04
HCN	H–C	0.97	0.97	0.98	0.93	0.92
	C–N	3.15	3.11	3.12	3.06	3.12

Table 2 Mayer bond orders for a set of simple di- and triatomic main group molecules calculated using ADF. All calculations used frozen cores

Method Basis set		LDA dz	LDA tz	BP86 dz
H_2		1.00	1.00	1.00
CO		2.16	2.32	2.31
CO_2		1.81	1.99	1.98
N_2		2.55	2.89	2.87
N_2O	N–N	2.15	2.49	2.47
	N–O	1.49	1.70	1.68
F_2		0.98	0.73	0.73
HF		0.88	0.44	0.47
H_2O		1.01	0.95	0.95
HCN	H–C	0.91	0.98	0.98
	C–N	2.67	3.01	2.99

Table 3 Mayer bond orders for a set of simple polyatomic main group molecules calculated using Gamess-UK

Method Basis set		LDA cc-pvdz	BP86 cc-pvdz	B3LYP cc-pvdz	B3LYP tzvp	B3LYP cc-pvtz
CH_4		0.99	1.00	1.00	0.97	0.97
CF_4		1.27	1.24	1.22	1.17	1.23
CCl_4		1.06	1.04	1.04	1.09	1.06
C_2H_2	C–H	1.04	1.05	1.05	0.97	0.93
	C–C	2.71	2.68	2.70	2.85	2.82
COH_2	C–H	0.91	0.91	0.92	0.90	2.12
	C–O	2.23	2.21	2.20	2.09	0.97
C_2H_6	C–H	0.97	0.97	0.98	0.97	0.97
	C–C	1.12	1.11	1.10	0.97	0.95
C_6H_6	C–H	0.93	0.94	0.95	0.98	0.97
	C–C	1.46	1.45	1.45	1.39	1.38
CH_3OH	C–H	0.97	0.97	0.97	0.96	0.95
	C–O	1.11	1.09	1.07	0.96	1.01
	O–H	1.00	1.01	1.01	0.92	1.02
CH_3CN	C–H	0.94	0.94	0.95	0.95	0.95
	C–C	1.05	1.08	1.07	0.97	0.98
	C–N	3.24	3.18	3.20	3.05	3.26
B_2H_6	B–H_t	0.97	0.97	0.98	0.99	0.98
	B–H_b	0.46	0.47	0.47	0.47	0.48
	B–B	0.75	0.70	0.67	0.60	0.54
BH_3NH_3	B–H	0.98	0.98	0.98	0.99	0.98
	B–N	0.80	0.77	0.75	0.57	0.62
	B–N	0.97	0.98	0.98	0.90	0.97
PH_3		0.83	0.83	0.83	0.85	0.87
SO_4^{2-}		1.60	1.58	1.56	1.57	1.70

Table 4 Mayer bond orders for a set of simple polyatomic main group molecules calculated using ADF. All calculations used frozen cores

Method Basis set		LDA dz	LDA tz	BP86 dz
CH_4		0.99	0.99	1.00
CF_4		0.83	0.58	0.56
CCl_4		1.04	1.10	1.08
C_2H_2	C–H	1.04	1.08	1.09
	C–C	2.18	2.71	2.68
COH_2	C–H	0.91	0.95	0.95
	C–O	1.75	1.94	1.93
C_2H_6	C–H	0.98	1.02	1.02
	C–C	0.96	0.90	0.88
C_6H_6	C–H	1.04	1.06	1.06
	C–C	1.24	1.38	1.37
CH_3OH	C–H	0.97	0.99	0.99
	C–O	0.81	0.87	0.85
	O–H	1.02	1.00	0.99
CH_3CN	C–H	0.95	0.97	0.98
	C–C	0.92	1.04	1.02
	C–N	2.62	2.96	2.93
B_2H_6	B–H_t	0.99	0.92	0.89
	B–H_b	0.47	0.49	0.49
	B–B	0.28	0.47	0.44
BH_3NH_3	B–H	0.97	0.92	0.90
	B–N	0.50	0.56	0.55
	B–N	0.96	1.02	1.03
PH_3		0.92	0.93	0.93
SO_4^{2-}		1.48	1.56	1.53

present, however, significant bond orders may result for atom pairs which are not normally labelled as bonded.

The calculations suggest that the bond order is insensitive to the density functional method employed. Larger dependence on the size and quality of the basis set is observed however. The bond orders calculated using GTOs with the Gamess-UK code appear to be larger than those obtained using STOs with ADF. The correlation consistent (cc) basis set available for GTO based programs is of high quality and there appears to be little difference in the bond orders produced using the cc basis sets of double- and triple-ζ quality (cc-dzvp and cc-tzvp respectively). The performance of the triple-ζ GTOs and STOs (tzvp and tz respectively) appears to be similar. The frozen cores used in the ADF calculations lead to slightly smaller bond orders in most cases.

In contrast, there are noticeable variations in the performance of the double- and triple-ζ STOs (dz and tz respectively). The dz basis set appears to perform especially poorly for systems with pronounced anisotropy in the bonding. The multiplicities of the C–O bond in CO and CO_2, the N–N and N–O bonds in N_2O and the C–N bond in CH_3CN and HCN are predicted to be much smaller with the dz basis.

The bond orders predicted for X–F bonds appear to be very sensitive to the basis set and represent the largest differences between the GTO and STO results. In the GTO calculations, the H–F bond order varies between 0.91 and 1.06 and this corresponds to fluorine Mulliken charges of −0.36 and −0.20 respectively. In the STO calculations, the H–F bond order varies between 0.44 and 0.88 corresponding to fluorine Mulliken charges of −0.74 and −0.43 respectively. A very low bond order is predicted by the tz functions and thus corresponds to considerably higher ionicity in the bond than that from the other calculations. The C–F bonding in CF_4 shows similar behaviour with fluorine Mulliken charges of *ca.* −0.1 predicted by the GTO basis sets leading to bond orders greater than one and fluorine Mulliken charges of *ca.* −0.6 predicted by the tz STO basis set leading to bond orders close to 0.5. The same variations are not evident for the C–Cl bond in CCl_4.

As discussed above, it is possible to learn more about the bonding in a molecule by decomposing the bond order into the contributions from molecular orbitals of different symmetry

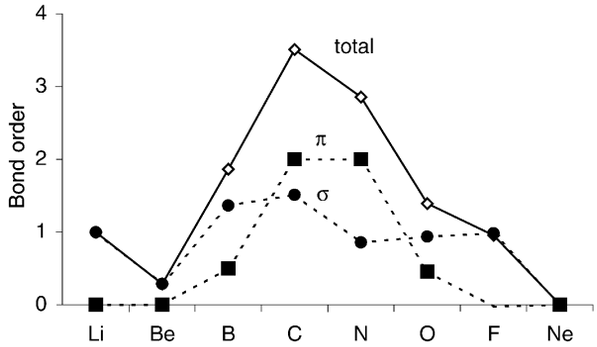

Fig. 1 Bond orders for the homonuclear diatomics of the first row. The total bond order (full line) is broken down into the contributions (broken lines) from the σ and π orbitals.

types. To illustrate this, the bond orders for the homonuclear diatomics of the first row elements are shown in Fig. 1 together with the σ and π contributions calculated using the DeFT program and the tzvp basis functions. The bond orders in these molecules are very similar when calculated with different basis sets. The bonding in these molecules is, of course, well understood and, indeed, forms the subject of many introductory courses in molecular orbital theory. The values shown in Fig. 1 are not, however, equal to those given by simple electron counting.[21] The possibility of s–p mixing in these systems changes the character of the σ_g and σ_u orbitals. This mixing has effects other than the well-known changes in the energetic ordering of $3\sigma_g$ and $1\pi_u$ between N_2 and O_2. The $2\sigma_g$ and $3\sigma_g$ orbitals in these molecules, in the absence of s–p mixing, result from the in-phase overlap of the 2s and $2p_z$ atomic orbitals respectively. Inclusion of s–p mixing lowers the energy of $2\sigma_g$ at the expense of reducing or removing the bonding character of $3\sigma_g$. The $2\sigma_u$ and $3\sigma_u$ orbitals, in the absence of s–p mixing, are antibonding as a result of the out-of-phase overlap of the 2s and $2p_z$ orbitals respectively. Inclusion of s–p overlap raises the energy of $3\sigma_u$ by the mixture of some bonding character into $2\sigma_u$. Be_2 with a valence configuration of $(2\sigma_g)^2(2\sigma_u)^2$ is isoelectronic to He_2 and so simple counting predicts a bond order of zero. Unlike helium however, Be has sufficiently low lying p-orbitals for a small net bond order to result from the mixing of p-character into the occupied levels. Similarly, B_2 which has a valence configuration $(2\sigma_g)^2(2\sigma_u)^2(1\pi_u)^2$ is not simply π-bonded but has an important σ-component.

The electronic configurations of the C_2 and N_2 molecules differ only in the occupation of the $3\sigma_g$ orbital. The π-bond order is 2 for both systems. If s–p mixing is neglected, the $3\sigma_g$ orbital is strongly bonding and leads to the classical bond orders of 2 and 3 for C_2 and N_2 respectively. The result of s–p mixing is that the $3\sigma_g$ orbital is essentially non-bonding so that the bond orders of N_2 and N_2^+ are essentially the same. The increased s–p gap in N_2 compared to B_2 and C_2 actually leads to a decrease in the importance of s–p mixing in the $2\sigma_g$ and $2\sigma_u$ orbitals so N_2 is actually predicted to have a smaller σ-component.

s–p mixing thus leads to non-integer values for the bond orders even in these two-centre, unpolarized molecules and a distinct asymmetry in the σ-bond orders across the series. This is not the case for the π-bonding which is unaffected by the mixing and has the expected mirror symmetry between the two halves of the p-block.

As discussed above, a full breakdown of the bond order into its components from different symmetry types is achievable when one of the atoms is at the centre of the molecule. This is the case for the tetrahedral molecules in Tables 3 and 4. Thus, the C–H bond order in methane is calculated to be 1.00 at the B3LYP/cc-pvdz level and this corresponds to 0.25 and 0.75 from the a_1 and t_2 components respectively. This is exactly as expected for a purely σ-bonded molecule with the bonding

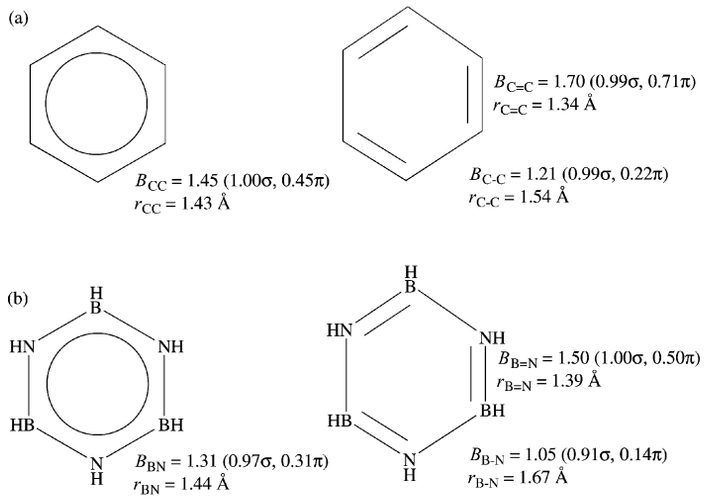

Fig. 2 σ and π-bond orders and dimensions for (a) benzene and (b) borazine with regular and distorted structures.

divided equally between the carbon s-orbital (a_1) and each of the three p-orbitals (t_2). The same calculation level gives a C–F bond order of 1.22 in CF_4 with contributions of 0.24 from a_1 and 0.92 from t_2 with the small residual component arising from e symmetry orbitals containing carbon d polarization functions. The increased t_2 contribution relative to CH_4 results from π-like bonding involving the fluorine lone-pairs. The C–Cl bond order in CCl_4 is calculated to be 1.04 with contributions of 0.20 from a_1 and 0.81 for t_2 which is consistent with weaker σ-bonding than in CH_4 with a smaller π-contribution than in CF_4. Whilst the ADF bond orders for these systems are somewhat smaller than these values, the breakdown leads to similar conclusions.

The STO LDA/tz and GTO B3LYP/tzvp calculations both suggest some multiple bond character for the S–O bond in SO_4^{2-}. The bond order for both is 1.56 which should be compared to the value from valence bond considerations of 1.5. The breakdown is very similar from the two calculations and gives contributions of 0.25 from a_1, 1.15 from t_2 and 0.16 from e. This molecule is isoelectronic to CF_4 and CCl_4 and the small contribution from the sulfur 3d functions is evident in the enhanced e orbital component in SO_4^{2-}. The largest differences occur in the t_2 orbitals where multiple S–O bonding results from the larger S 3p orbitals.

As discussed above, a complete breakdown of the bond orders for the C_6H_6 molecule is not possible. However, there is a complete separation of the atomic orbitals involved in the in-plane and out-of-plane interactions and it is thus possible to calculate the contributions from these 'σ' and 'π' components. The B3LYP/cc-pvdz C–C bond order of 1.45 is produced from σ and π contributions of 1.00 and 0.45 respectively. The π bond order can be compared to the value from Hückel theory of 0.67. Illuminating comparison can be made with the values for heterocycles.[4d,e] In borazine, for example, the B–N bond order is 1.31 with σ and π contributions of 0.97 and 0.31 respectively. The effect of the bond polarization is evident in the π component in particular.

The idea that the regular hexagonal structure of benzene is a result of the σ-framework and that the π bonding actually favours localization has been developed by Shaik and coworkers[22] using a variety of computational strategies. Fig. 2(a) shows the bond orders calculated for benzene with the observed D_{6h} structure and that for a Kekulé form of benzene with bond lengths corresponding to single and double C–C bonds. In the latter form, the calculations predict considerable localization of the π-bonding. The longer C–C connections have greatly reduced π-bond order compared to the symmetrical structure whilst it is enhanced for the short C–C bonds. The total π-bond order obtained by adding up the contributions from the six C–C connections around the ring *increases* as the structure is distorted from 2.70 to 2.79 as the character of the π-orbitals change. Lowering of the symmetry from D_{6h} to D_{3h} allows mixing between the occupied and virtual π-orbitals leading ultimately to complete localization. Their form is optimal in the distorted geometry, although the changes are clearly small. The σ-bond orders show much smaller changes. Decreasing the C–C bond from the single to the double bond length makes little difference to the form of the in-plane orbitals. The total C–C σ-bond order for the six bonds in the ring decreases from 6.00 to 5.94. Although the changes in the individual and total π and σ-bond orders are small, they are consistently reproduced by the different levels of theory.

Borazine also has a regular hexagonal structure but, as outlined above and discussed in detail elsewhere,[4e] the π bonding is considerably weaker than in benzene. Fig. 2(b) shows the bond orders for regular (D_{3h}) and distorted (C_{3h}) borazine. The structure of the latter has alternating B–N 'single' and 'double' bond lengths taken from BH_3NH_3 and from the optimized structure of the ethene analogue BH_2NH_2 respectively. The total B–N σ-bond order decreases from 5.82 to 5.72 and the total π-bond order *increases* from 1.86 to 1.92 as the molecule is distorted. It should be noted that the increase in the π-bonding occurs even though the distortion is such that the bond lengthening is much greater than the bond shortening. The results are consistent with a distortive π system.

(b) Pseudo-aromatic S–N rings

The diagonal relationship between sulfur and nitrogen in the periodic table leads to similarities in their electronegativities and coordination numbers. The N–N and N–O single bonds are relatively weak, probably as a result of the repulsion between lone pairs on the atoms of the intrinsically short bonds, and catenation is limited in nitrogen and nitrogen–oxygen chemistry. The S–S and S–N bonds, however, are much longer and formation of chains, rings and clusters is possible. Whilst S–S bonds are found in puckered rings and clusters, the lower electron count of the S–N connection means that multiple bonding is possible leading to similarities with the chemistry of both S–S and C–C bonds. The small differences in electronegativities between sulfur and nitrogen and the greater polarizability of the larger sulfur atom leads to significant differences in the structural chemistry. Tetrasulfur tetranitride, S_4N_4, adopts the cradle conformation[23] with D_{2d} symmetry shown in Fig. 3(a). The structure has a number of interesting characteristics. The S–N bond length of 1.62 Å is significantly shorter than the sum of the covalent radii suggesting multiple bond character. The transannular S–S distance of 2.58 Å is longer than the S–S

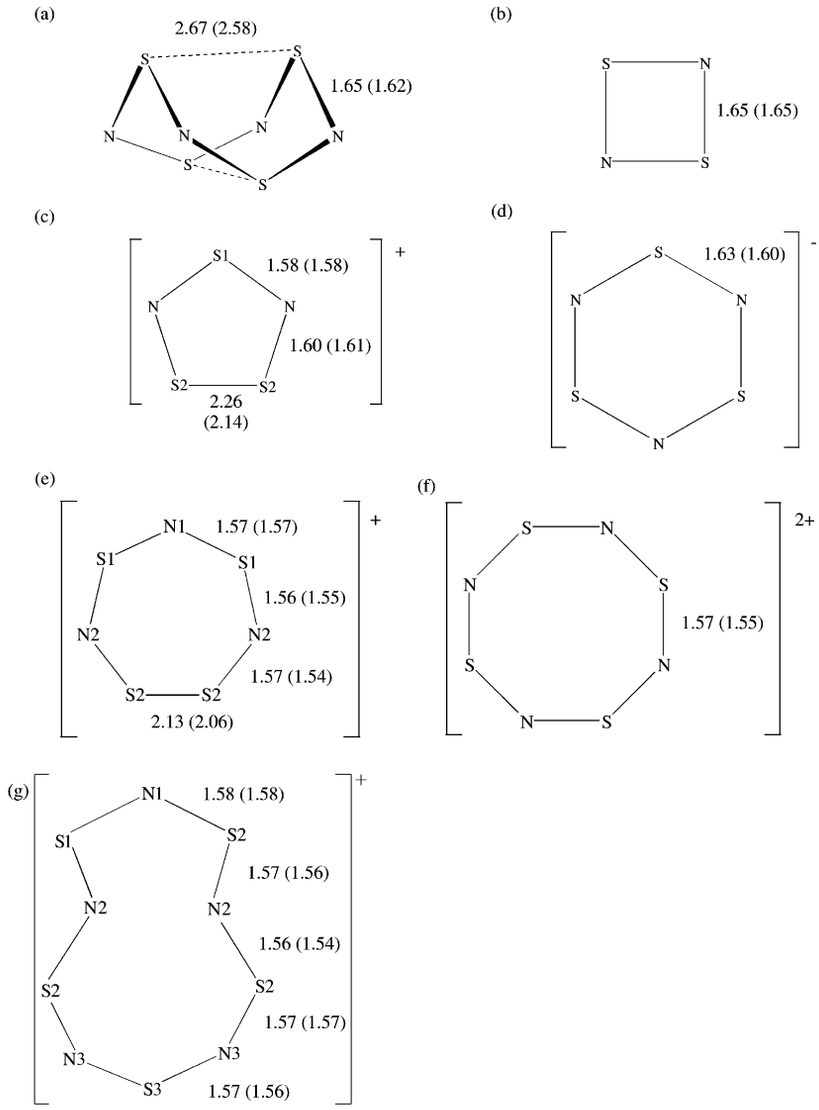

Fig. 3 Optimized structures for the sulfur–nitrogen heterocycles (a) S_4N_4, (b) S_2N_2, (c) $S_3N_2^+$, (d) $S_3N_3^-$, (e) $S_4N_3^+$, (f) $S_4N_4^{2+}$ and (g) $S_5N_5^+$. The structural parameters determined experimentally are shown in parentheses.

distance in elemental sulfur but shorter than twice the sulfur van der Waals radius suggesting a degree of covalent bonding.

Fig. 3(a) also shows the optimized structure obtained with a B3LYP calculation using Gaussian98 and a 6-311G(3d,3pd) basis. Table 5 lists the S–N and S–S bond orders and the S Mulliken charge for this calculation. These parameters are also listed for B3LYP calculations with different basis sets and for calculations using a tzvp basis sets with different exchange-correlation functionals.

The S–N and S–S bond orders vary between 0.91 and 1.35 and between 0.22 and 0.56 respectively for different basis sets. There are also significant variations in the sulfur Mulliken charges from the different basis sets. As noted above for the classical main group molecules, there is little variation in these properties when the exchange-correlation functional is varied. The Pople 6-31G and 6-311G basis sets lead to higher sulfur atomic charge and lower bond orders. The addition of polarization functions to form the 6-311G(3d,3pd) leads to decreased sulfur charge and increased covalency. All but the 6-31G and 6-311G calculations suggest that the S–N bonds have multiple bond character. As outlined below, the values calculated using 6-31G and 6-311G in fact relate to the ionicity of the bonding predicted by these basis sets and do not preclude the existence of multiple bonding. The S–N 'σ-bonding' in this system is likely to have a bond order smaller than unity using these basis sets and this obscures the multiple bond character. Such

Table 5 S–N and transannular S–S bond orders and Mulliken charges for S_4N_4

Level		Bond order		Mulliken charge q_s
		S–N	S–S	
B3LYP	6-311G(3d,3pd)	1.35	0.48	+0.34
B3LYP	cc-pv5z	1.18	0.56	+0.51
B3LYP	STO-3G	1.09	0.22	+0.50
B3LYP	6-31G	0.91	0.22	+0.79
B3LYP	6-311G	0.91	0.41	+0.73
B3LYP	tzvp	1.10	0.55	+0.64
SVWN	tzvp	1.11	0.48	+0.60
BP86	tzvp	1.11	0.48	+0.60
BLYP	tzvp	1.11	0.47	+0.61
B3P86	tzvp	1.09	0.50	+0.63

multiple bonding is often ascribed to the role of S–N d_π–p_π bonding. As well as allowing decomposition of the bond order by orbital symmetry type, the form of the Mayer bond order also allows the contribution from the atomic orbitals on the atoms to be gauged. The sulfur d-orbital contribution to the S–N bond order using the 6-311G(3d,3pd), cc-pv5z and tzvp basis sets are calculated to be 0.28, 0.20 and 0.15 respectively indicating a small role for these functions. The remaining basis sets do not include d-functions on the atoms.

All the calculations indicate that there is genuine S–S

Table 6 S–N bond orders, atomic charges and AIM bond ellipticity (ε) for S_2N_2. π-bond orders are given in parentheses and the missing data indicates that the AIM calculations did not converge

		S–N bond order			S atomic charge		
Level		Mayer	AIM	ε	Mulliken	NBO	AIM
B3LYP	6-311G(3d,3pd)	1.38 (0.36)	1.28	0.39	+0.68	+0.88	+1.13
B3LYP	cc-pv5z	1.21 (0.33)	1.27	0.39	+0.71	+0.89	+1.17
B3LYP	STO-3G	1.20 (0.23)	—	0.14	+0.45	+0.42	—
B3LYP	6-31G	1.06 (0.23)	1.41	0.39	+0.73	+0.84	+0.96
B3LYP	6-311G	1.06 (0.25)	1.42	0.36	+0.68	+0.78	+0.91
B3LYP	tzvp	1.19 (0.29)	1.24	0.46	+0.63	+0.84	+1.21
SVWN	tzvp	1.19 (0.29)	1.26	0.41	+0.60	+0.81	+1.13
BP86	tzvp	1.18 (0.29)	1.25	0.44	+0.60	+0.81	+1.18
BLYP	tzvp	1.19 (0.28)	1.25	0.43	+0.60	+0.82	+1.16
B3P86	tzvp	1.18 (0.27)	1.23	0.48	+0.62	+0.83	+1.25

transannular bonding. Given the complexity of the molecular orbitals for this molecule, the bond order is a valuable tool for condensing the bonding and antibonding contributions made by the occupied levels to the interaction.

The dependence of the Mulliken charge and Mayer bond order on the basis set, displayed in S_4N_4 and the classical main group molecules discussed earlier, is clear. Large variations in Mulliken charges have, of course, been noted before.[24] The relationship between the Mulliken charge and the form of the Mayer bond order given in eqn. (8) is evident from their definitions and it is clear that similar precautions are required when comparing bond orders for different molecules. For the Mayer bond order to be useful, however, requires that the *variations* between related molecules *are* reproduced by different basis sets.

Fig. 3(b–g) show optimized geometries for the known binary sulfur–nitrogen planar ring systems. The optimized structures were obtained using the 6-311G(3d,3pd) basis set at the B3LYP level using Gaussian98 and are compared with the experimentally determined geometries[25] in Fig. 3. Excellent agreement between calculated and observed structures is found. A number of the experimental structures possess lower symmetries than those predicted by the calculations with, for example, small alternations in S–N distances around the rings. In all cases, the DFT stuctures were optimized from low symmetry starting points. The $S_4N_3^+$ ring, for example, is predicted to have C_{2v} symmetry from the calculations on the free ion. It appears that solid state effects are responsible for the observed distortions rather than any electronic factors intrinsic to the rings.

Fig. 4 shows the variation in the sulfur atomic charge for the rings with ring size using six different basis sets calculated at the B3LYP level. For the rings containing inequivalent sulfur atoms, average values are plotted in Fig. 4. Three methods of determining atomic charge have been used: Mulliken, NBO and AIM. Calculations have also been performed using the same basis sets with different exchange-correlation functionals. Table 6 shows the variation in the sulfur charge in S_2N_2 as an illustration of the dependence on density functional. The results for the other ring systems show very similar behaviour.

The Mulliken and NBO charges are found to show little sensitivity to the density functional employed. The variation in the AIM charge is somewhat larger but is still within ± 0.1 e^-. The NBO charges are found to be larger than the Mulliken values whilst the AIM charges are significantly larger than both. With the exception of the STO-3G results, the NBO charge is found to be relatively insensitive to the basis set and the variation with ring size is well reproduced by all of the basis sets. The NBO charges for the minimal basis set are markedly lower than those for the larger sets although the overall variation with ring size is reproduced. The dependence of the Mulliken charges on basis set is, as expected, much larger than that found using the NBO prescription. Meaningful comparison between the Mulliken charges calculated using different basis sets is clearly not possible. The variation between the rings is, however, reproduced by all of the basis sets, at least qualitatively. The AIM charges show similar dependence to the Mulliken charges on the basis sets although there were convergence problems with the STO-3G basis set so that it is not possible to gauge the performance of the minimal set. It should be noted that the three definitions of atomic charge predict the *same* dependence of the sulfur charge on the ring charge despite

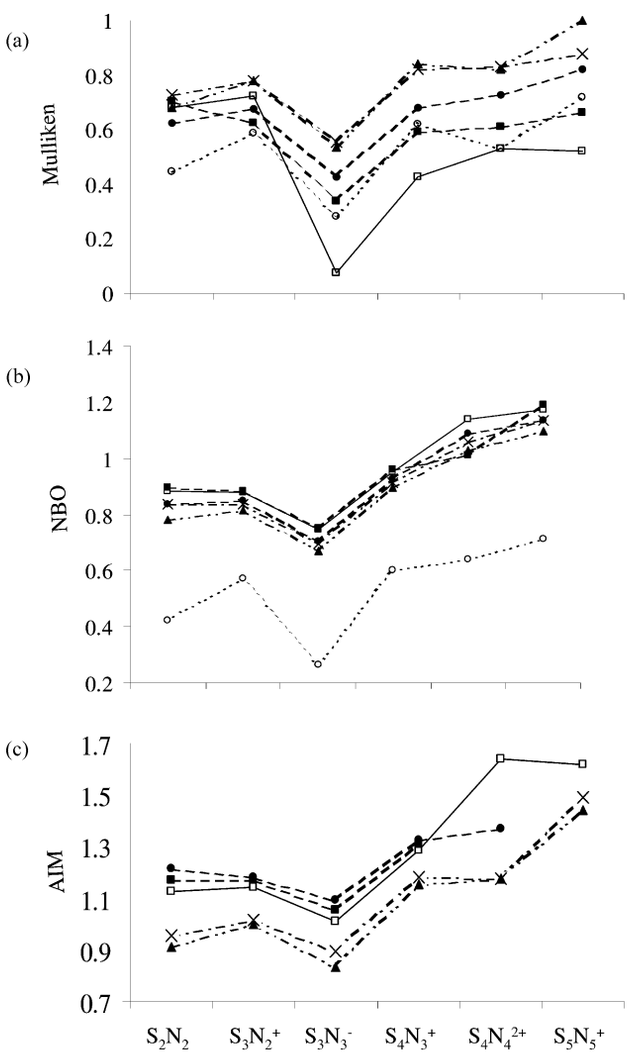

Fig. 4 Variation in the (a) Mulliken, (b) NBO and (c) AIM sulfur atomic charge for the sulfur–nitrogen rings with ring size at the B3LYP level using the basis sets 6-311G(3d,3pd) (symbol □), cc-pv5z (symbol ■), STO-3G (symbol ○), 6-31G (symbol ×), 6-311G (symbol ▲) and tzvp (symbol ●).

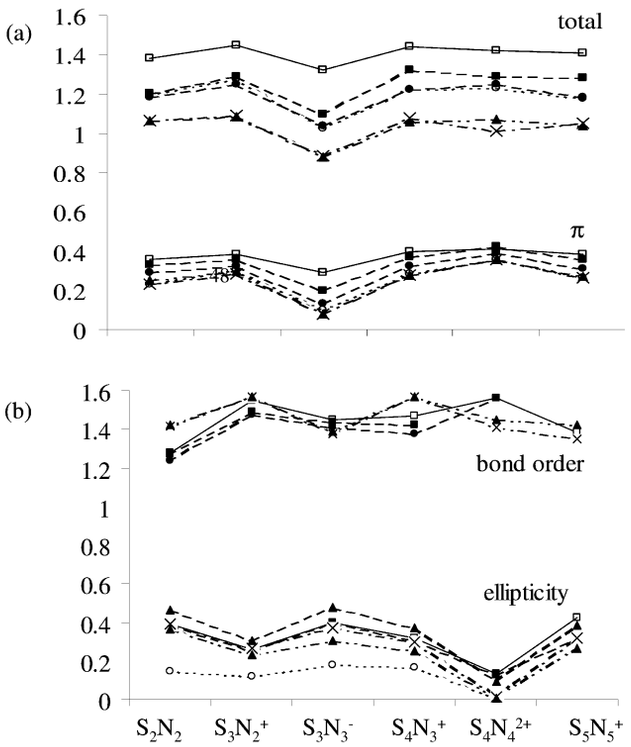

Fig. 5 Variation in the (a) Mayer total and π-orders and (b) AIM bond orders and ellipticity values for the sulfur–nitrogen rings with ring size at the B3LYP level using the basis sets 6-311G(3d,3pd) (symbol □), cc-pv5z (symbol ■), STO-3G (symbol ○), 6-31G (symbol ×), 6-311G (symbol ▲) and tzvp (symbol ●).

quantitative differences and variations with basis set. The sulfur atom is positively charged in each ring. As shown in Fig. 4, there is a general trend for the sulfur charge to increase with ring size with the exception of $S_3N_3^-$. As sulfur is less electronegative than nitrogen, the bonding orbitals have greater N character whilst the antibonding orbitals have greater S character. Enlargement of a ring with an extra sulfur atom adds two electrons and one p_π orbital whereas an extra N atom contributes one electron and one p_π orbital. As the rings get larger, therefore, the number of the π-orbitals that are unoccupied increases. Thus S_2N_2 has one, $S_4N_3^+$ has two and $S_4N_4^{2+}$ and $S_5N_5^+$ have three unoccupied π-levels respectively. As the highest occupied levels are antibonding in character for these electron-rich rings, the sulfur charge thus reduces with ring size. The anionic $S_3N_3^-$ ring is an exception as its charge leads to the same number of unoccupied π levels as S_2N_2.

Fig. 5 shows the variation in the S–N bond order for the same rings and basis sets. It includes bond orders calculated using the Mayer definition and the AIM approach. For the rings containing several inequivalent S–N connections, average values are shown in Fig. 5. The Mayer bond orders are decomposed into in-plane and π components. The AIM ε parameter is also included. This is the ellipticity of the electron density at the bond critical point[26] and is interpreted as an indicator of the π character of a bond. Table 6 also lists the bond orders for S_2N_2 calculated using different density functionals. The dependence of the bond orders on the nature of the functional is very similar for the other rings.

The S–N Mayer bond orders show similar sensitivity to the basis sets as noted above for the cradle S_4N_4 and the classical main group systems. However, the variation in the bond order with ring size is accurately reproduced by all of the basis sets. The decomposition reveals moreover that the sensitivity of the π bond order on the basis sets is much smaller than that of the in-plane component. As found for the S_4N_4 cluster, the Pople 6-31G and 6-311G basis sets predict bond orders which are much smaller than those from the other bases. The π orders for the Pople basis sets are, however, in line with the others and it appears to be the in-plane values which are unusually small. This can be related to the larger Mulliken charges given by these basis sets. The lack of d-orbitals in these basis sets does not significantly effect the description of the π-bonding.

As suggested by the atomic charges and the discussion above, the bond order in $S_3N_3^-$ is lower than in the other rings as a result of the π electron count. For the other rings, there is a general increase in the π bond order across the series as the number of empty π* levels increases. The two largest rings, $S_4N_4^{2+}$ and $S_5N_5^+$, both have three empty π levels. The sulfur and nitrogen atoms in the D_{4h} $S_4N_4^{2+}$ ion are on different C_2 axes. This ensures that the two highest occupied π-orbitals are either nodal on the sulfur or nitrogen atoms and are non-bonding. The C_{2v} symmetry of $S_5N_5^{2+}$ means, however, that there is sulfur and nitrogen character in all of the π-orbitals and that the highest occupied levels are S–N antibonding. The bond order in the $S_4N_4^{2+}$ ring is thus higher. There is a similar pattern in the S_2N_2 and $S_3N_3^-$ rings which both have one empty π* level. The D_{2d} symmetry of the S_2N_2 ring ensures that the two highest occupied orbitals are nodal at either S or N and are non-bonding. The D_{3h} symmetry of $S_3N_3^-$, however, leads to sulfur and nitrogen character in all of the orbitals and the highest occupied levels are strongly antibonding.

The AIM bond orders broadly reflect the Mayer values although, like the atomic charges, are generally larger. The AIM ellipticity values are all greater than zero indicating that the electron density in the centre of the S–N bond is elongated in one direction, such as by π bonding. Although varying in magnitude, the ε values vary with ring size consistently for the different basis sets. The link with the π bonding is less clear, however, and comparison between the Mayer or AIM bond orders and the ε values suggest that there is an inverse relationship between them.

The calculations on the S–N rings again show that the Mayer bond order, like the Mulliken charge, has a strong basis set dependence and thus their values cannot in any way be considered absolute. However, their computational value arises through their ability to condense information from delocalized molecular orbitals into local form. Trends in bonding interactions are reproduced irrespective of basis set variations. The direct link with the molecular orbitals means that the effects of the molecular symmetry and electron count can be related to the localized atomic charges and atom–atom bond orders.

(c) Mixed halogen and hydrogen peroxide isomers

Halogen oxides are now known to play a significant role in the catalytic depletion of stratospheric ozone. Stratospheric chlorine atoms mainly result from the release of chlorofluorocarbons (CFCs) whilst the level of bromine is due to a variety of natural and man-made sources including organisms in seawater and solvents such as methyl bromide. Halogen atoms in the atmosphere react with ozone to form halogen monoxides. Molina and Molina[27] proposed the self-reaction of ClO to form its dimer as a step in the catalytic destruction of ozone. This has led to a number of experimental and theoretical studies[28,29] on the chemistry and physical properties of Cl_2O_2 and it has been determined that the peroxide is the most stable isomeric form.

A number of experimental studies on the BrO self-reaction have also been reported[30] involving the short-lived BrOOBr intermediate. The study by Yung *et al.*,[31] however, showed that the most effective ozone depleting cycle involving bromine is probably one in which BrO reacts with ClO and Toohey and Anderson[32] proposed an intermediate [BrOOCl] to account for the observed reaction paths. As the OH radical is also present in the atmosphere, the analogous reactions of HO with ClO and BrO possibly through HOOX (X = Cl or Br) are also possible. HOOCl has been proposed[33] as an important stratospheric molecule.

We have previously reported[4c] calculations on the bonding and structure of the peroxide form of the dimer XOOX′ (X, X′ = H, F, Cl, Br and I). These molecules form a structurally and chemically diverse set and the electronegativity of the substituents has a large effect on the O–O bonding which varies between a double bond (FOOF) and a single bond (HOOH). A number of isomeric forms of these molecules are also possible intermediates in atmospheric processes and there have been a number of studies on the isomers of Cl_2O_2,[34] $ClBrO_2$,[35] $XBrO_2$ (X = H, Cl and Br),[36] Br_2O_2,[37] $ClIO_2$ [38] and I_2O_2.[39]

Calculations have been performed at the BP86 level using the DeFT code with double-ζ basis sets for the halogen and triple-ζ basis sets for oxygen and hydrogen to study the local minima on the potential energy surfaces of the $XX'O_2$ molecules and the bonding. Scheme 1 shows the important isomeric structures of

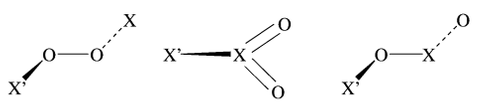

I **II** **III**

Scheme 1 Peroxide (**I**), Y-shaped (**II**) and head-to-tail (**III**) isomers of the mixed halogen peroxides $XX'O_2$ (X = H, F, Cl, Br and I, X′ = Cl, Br and I).

the $XX'O_2$ molecules. The X′OOX structure (**I**) represents the skewed peroxide, $X'XO_2$ (**II**) corresponds to the non-planar, Y-shaped structure with C_s symmetry and X′OXO (**III**) is a head-to-tail isomer of the peroxide form. The oxidation state required for the connectivity in the central halogen position in the $X'XO_2$ and X′OXO structures restricted the study of these isomers to the molecules with X = Cl, Br and I. Calculations on the fourth isomeric form, OXXO, suggested that these are highly unstable. Calculations were also performed on the fragmentation products from these molecules: XO, XO_2, OXO and XX′O. The calculated structures of these molecules are deposited as supplementary material.†

As outlined above, Lendvay[7] has shown that the Mayer bond order for C–C, C–H and C–O bonds correlates very well with bond length using function (9) due to Pauling and co-workers.[6] The halogen–oxygen bonds are a more severe test as they vary over wide ranges in the compounds studied depending on the formal oxidation state and on the electronegativity of the attached groups. Fig. 6(a–d) shows the correlation obtained for the halogen–oxygen bonds for the systems in Scheme 1. Table 7 lists the fitting parameters required and the sum of squares error for each bond type.

As can be seen in Fig. 6, eqn. (9) describes the correlation quite well. The value of r_0 in the correlation function is the theoretical single bond order. The bond orders show the largest values for the most electropositive halogen, iodine, with a number of systems showing multiple bond character. Our previous report on the bonding in the peroxide forms[4c] showed the complexity of the bonding in these electron rich systems and the role of the halogen and oxygen 'lone-pairs'. Such an analysis was possible because of the reasonably high C_2 symmetry of the peroxide form. The other isomeric shapes shown in Scheme 1 have lower symmetry and such a treatment is less revealing. The usefulness of the bond order is that it combines the contributions to each bond from the many delocalized orbitals.

For the $(ClO)_2$, $(BrO)_2$ and (BrO)(ClO) dimers, previous computational studies[34–36] have concluded that the peroxide form is the most stable. Fig. 7 shows the relative energies of the iodine containing systems, XIO_2 (X = H, F, Cl, Br and I), for the isomeric forms shown in Scheme 1. For the systems with the heavier halogens, in particular, the calculations predict that the several isomers are close in energy to the ground state so that interconversions are possible. The relative energies of possible

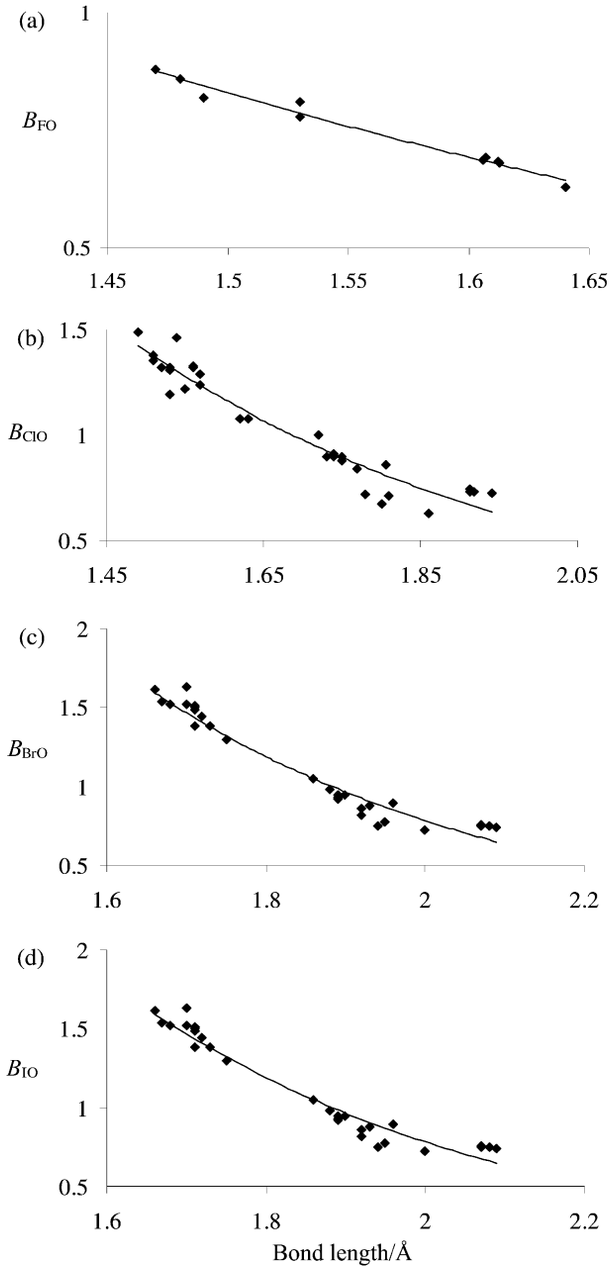

Fig. 6 Correlation between halogen–oxygen bond order and length for (a) F–O, (b) Cl–O, (c) Br–O and (d) I–O in the mixed hydrogen and halogen peroxide isomers.

Table 7 Fitted parameters for the correlation between bond order and bond length for the halogen–oxygen bonds in the $XX'O_2$ isomers. SSE is the sum of the squares error

Bond	r_0	b	SSE
F–O	1.396	0.586	0.002
Cl–O	1.687	0.542	0.16
Br–O	1.879	0.451	0.14
I–O	2.054	0.420	0.17

fragments are also shown. The latter suggest that the easiest fragmentation patterns involve loss of halogen atoms rather than oxygen. The weakness of the halogen–oxygen bonds for the heavier halogens is evident. The energy of the ground state with respect to the XO + IO is largest for X = H and F and is very similar for the remaining halogens. This suggests that the equilibrium constants for the IO self reaction and the IO/ClO and IO/BrO coupling reactions, which may be important in any atmospheric role, are likely to be similar.

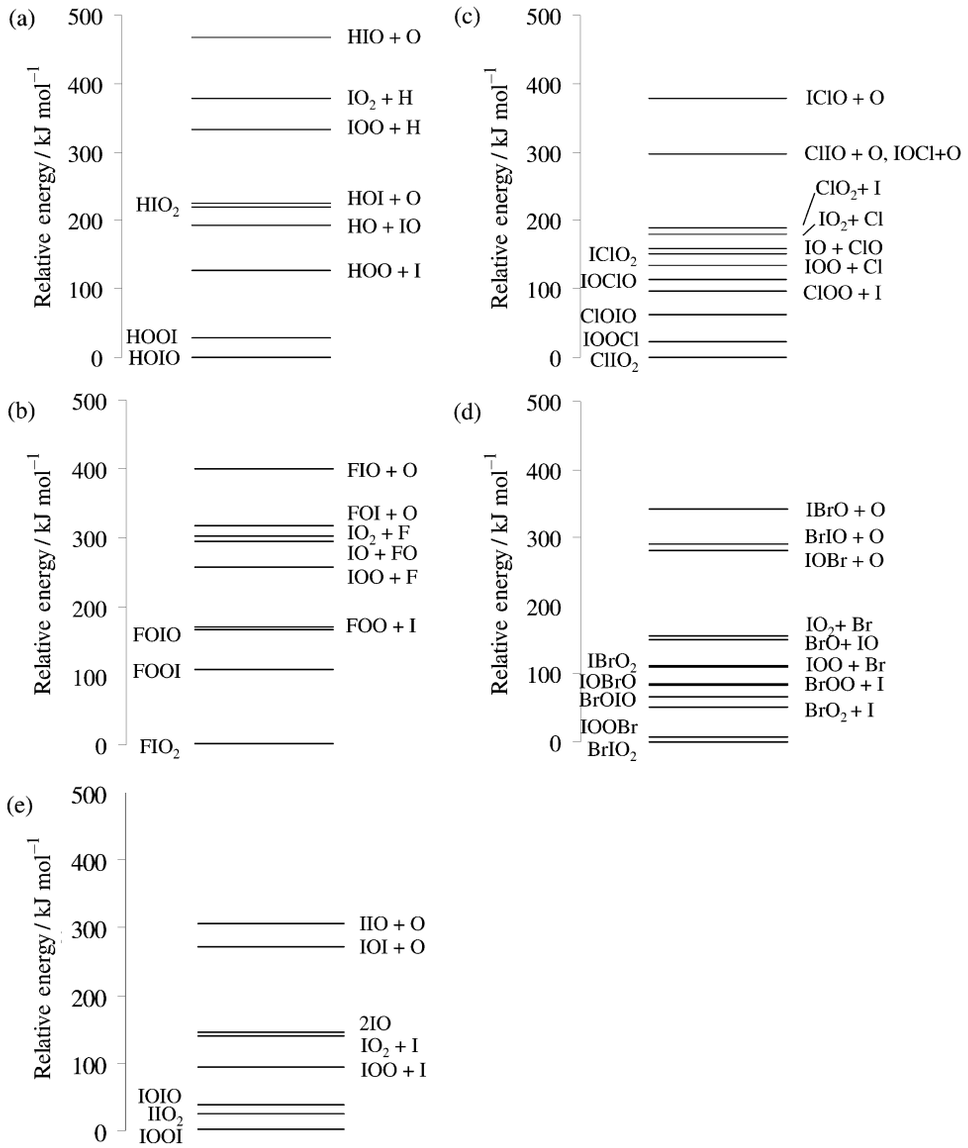

Fig. 7 Relative energies of the isomers of the XIO_2 system (X = H, F, Cl, Br and I) and the fragmentation products for (a) HIO_2, (b) FIO_2, (c) $ClIO_2$, (d) $BrIO_2$ and (e) IIO_2.

The Y-shaped XIO_2 and head-to-tail XOIO isomers contain hypervalent iodine. The calculations predict that these isomers are much more stable in the iodine systems than in the $(ClO)_2$, $(BrO)_2$ and (BrO)(ClO) dimers studied previously. The relative stability of the Y-shaped XIO_2 isomer increases with the electronegativity of X and is predicted to be the ground state for the (FO)(IO), (ClO)(IO) and (BrO)(IO) systems. This isomer contains a formally 5-valent iodine atom and the I–O bond orders are 1.73, 1.66, 1.63, 1.61 and 1.61 for X = F, Cl, Br, I and H respectively clearly indicating their multiple bond character. The inductive withdrawal of electron density by electronegative X enhances the covalency of the I–O bond leading to its observed shortening and strengthening. The XOIO isomer contains a formally 3-valent iodine atom and the XO–IO and XOI–O bond orders are around 1.6 and 0.8 respectively with little variation due to X. In both isomers featuring hypervalent iodine atoms, the terminal I–O bond orders are consistent with multiple bond character. In the analogous systems containing hypervalent chlorine and bromine, Fig. 7 reveals the lower multiplicity of the bonding and this leads to greater stability for the peroxide isomer.

(d) 3d Transition metal dichlorides

The geometries and electronic structure of the gas-phase 3d transition metal dichloride molecules have been the subjects of numerous studies.[40] The electronic structure of these apparently simple systems is interesting as they provide a severe but historically unexpected test of ligand-field theory and simple molecular orbital approaches.[5] Fig. 8 shows the crystal-field splitting of the d-orbital splitting for a linear and octahedral complexed transition metal. The magnitude of Δ_{oct} (equivalent to 10Dq) will no doubt be larger in the linear molecule due to the shorter bond lengths possible in the less crowded system but the pattern and relative energies are determined in an *ab initio* model such as crystal-field theory by the geometry alone.

Removal of the equatorial ligands from the octahedron stabilizes $d_{x^2-y^2}$ and d_{xy} leading to the low energy δ_g pair. To retain the baricentre, the energy of d_{z^2} and, to a lesser extent, the d_{xz} and d_{yz} pair rises. The former becomes the high energy σ_g function and the pair becomes the π_g functions. The predicted order is thus $\delta_g < \pi_g \ll \sigma_g$. Simple molecular orbital considerations[41] lead to the same order. The antibonding shift of the d-orbital with σ_g symmetry is larger than that of the π_g d-orbitals as a direct consequence of the expected dominance of ligand σ over π-donation. There are no low-lying orbitals of δ_g symmetry on common ligands so that the δ_g d-orbitals are non-bonding. Just as in other complexes of high-valent transition metal ions, the ground and low-lying excited terms arise from the population of these molecular orbitals which are

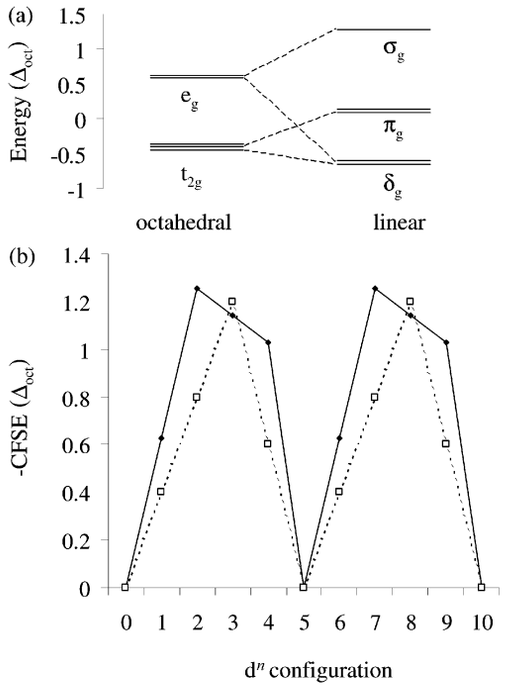

Fig. 8 (a) Crystal-field splitting and (b) crystal-field stabilization energy (CFSE) for a linear (◆) and octahedral (□) metal dichloride.

d-orbital in character. The assignment of the spectra of the dichloride molecules when first recorded were thus based on the d-orbital splitting $\delta_g < \pi_g \ll \sigma_g$.

More recent experimental[42,43] and theoretical studies[44,5b] of $NiCl_2$ and $CuCl_2$, however, have determined that their ground terms appear to arise from a d-orbital splitting pattern of $\delta_g < \sigma_g < \pi_g$. This ordering had previously been ruled out as it was thought to indicate that the ligands were acting as stronger π than σ-donors. Thus, the d^8 system $NiCl_2$ has a $^3\Sigma_g^-$ ground term arising from a $(\delta_g)^4(\sigma_g)^2(\pi_g)^2$ configuration rather than a $^3\Pi_g$ ground term resulting from $(\delta_g)^4(\pi_g)^4(\sigma_g)^1$. The same orbital ordering leads to a $^2\Pi_g$ ground term for $CuCl_2$ rather than the previously assumed $^2\Sigma_g^+$. These unexpected ground terms, and the reassignment of the electronic spectra they necessitate, were originally thought to indicate a failure of ligand-field theory. Our work[5] on $CrCl_2$, $FeCl_2$, $CoCl_2$ and $NiCl_2$, $CuCl_2$ and related systems such as transition metal monoxide molecules, however, has shown that the observed orbital ordering arises naturally when all ligand-field sources are included. For all these molecules, a reassignment of the ground state and excited states has resulted from a combined DF and ligand-field analysis.

Fig. 9 shows a qualitative molecular orbital diagram for a linear transition metal dichloride molecule. The orbitals which are mostly metal d-orbital in character are $1\delta_g$, $7\sigma_g$ and $2\pi_g$ and are shown in a box. As noted above, the $3d_\pi$ orbitals undergo an antibonding shift due to the interaction with the chloride $3p\pi_g$ combination whilst the $3d_\delta$ orbitals remain non-bonding. There are three valence functions of σ_g symmetry in the molecule that need to be considered: the metal $3d_\sigma$ and 4s orbitals and the chloride $3p\sigma_g$ orbital. Three molecular orbitals result from their combination: $6\sigma_g$, $7\sigma_g$ and $8\sigma_g$. The first and third are strongly bonding and antibonding respectively. The second orbital is approximately non-bonding and it is this orbital which is predominately $3d_\sigma$ in character. There is also appreciable metal 4s character in this orbital and we have previously described[5] the effective hybridization of these two metal functions to produce a hybrid which has its main part directed away from the metal–ligand axis. The hybridization leads to its non-bonding character. The ligand-field imposed on the $3d_\sigma$ orbital thus contains two distinct contributions: an antibonding interaction with the chloride lone-pairs and a stabilizing

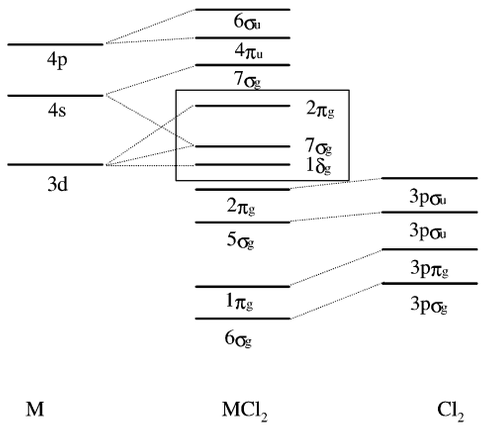

Fig. 9 Qualitative molecular orbital diagram for a linear 3d transition metal dichloride molecule. The ground and low lying excited terms arise from occupation of the metal 'd-orbitals': $1\delta_g$, $7\sigma_g$ and $2\pi_g$ shown in the box.

interaction with the higher lying 4s orbital on the metal. The d-orbital ordering of $\delta_g < \sigma_g < \pi_g$ thus does *not* necessarily signify that π-bonding is more important than σ-bonding.

Modern ligand-field theories[45] such as the angular overlap model (AOM) and cellular ligand-field model (CLF) aim to decompose the ligand-field into contributions from the σ and π nature of each ligands. The stabilization of the $3d_\sigma$ orbital must be included and this is modelled in two distinct but entirely analogous ways in the AOM and CLF approaches. In the former, the ligand-field source is seen as the metal 4s orbital and the extent of the stabilization is monitored with an extra parameter e_{ds} (sometimes labelled as σ_{ds}). The theoretical basis of the CLF model shows that the ligand-field arises from the orbitals built from ligand and metal (non d-) functions rather than the atomic orbitals themselves. The ligand-field source that stabilizes the $3d_\sigma$ orbital is the M–L σ* a_{1g} function which is built from the metal 4s with a small ligand component. This antibonding function is largest in the region around the metal *away* from the ligands and so is modelled with a 'void' cell and an e_{void} parameter. The rather different names for the parameter adopted by the two models masks the simple relationship between them and some have questioned the validity of the 'void' concept.[46] In reality the difficulty in the interpretation of the two parameters lies in their task of modelling a global (s-like) source within a localized bonding scheme. The d-orbital energies for a linear MCl_2 molecule in the AOM and CLF are,

$$\varepsilon(d_\sigma) = 2e_\sigma'(Cl) + 2e_{void} \quad \text{(CLF)} \qquad (14)$$

$$\varepsilon(d_\sigma) = 2e_\sigma'(Cl) - e_{ds} \quad \text{(AOM)} \qquad (15)$$

or

$$\varepsilon(d_\sigma) = 2e_\sigma \quad \text{(both)} \qquad (16)$$

$$\varepsilon(d_\pi) = 2e_\pi(Cl) \qquad (17)$$

$$\varepsilon(d_\delta) = 0 \qquad (18)$$

where eqn. (16) defines a new parameter as the sum of those in (14) and (15). The ground terms predicted for the molecules thus require $e_\sigma < e_\pi$. We have previously published successful CLF analyses[5] of the published spectra of $CrCl_2$, $FeCl_2$, $CoCl_2$, $NiCl_2$ and $CuCl_2$ within this revised parameterization scheme. The spectrum of VCl_2 has also been reported[47] and consists of a relatively intense peak at 14500 cm^{-1} and maxima at 9600 cm^{-1} and 10700 cm^{-1} on its low energy side. This spectrum leads to CLF $e_\sigma = 2400$ cm^{-1} and $e_\pi = 4940$ cm^{-1} and Racah $B = 200$ cm^{-1} in line with the values for $CrCl_2$. These parameter values lead to a reassignment of the band at 14500 cm^{-1} as

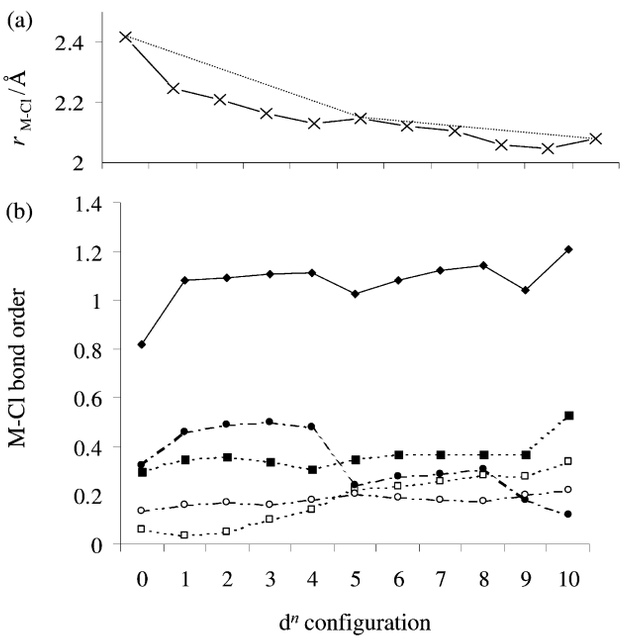

Fig. 10 (a) Bond lengths and (b) bond orders for the 3d transition metal dichlorides. The total bond orders (◆) are decomposed into the σ and π contributions (■ and □ for σ_g and σ_u respectively and ● and ○ for π_g and π_u respectively).

Table 8 Ground terms, strong-field configurations and bond lengths for the 3d transition metal dichloride molecules

MCl_2	Ground term	Configuration			Bond length/Å
		δ_g	σ_g	π_g	
$CaCl_2$	$^1\Sigma_g^+$	0	0	0	2.418
$ScCl_2$	$^2\Sigma_g^+$	0	1	0	2.244
$TiCl_2$	$^3\Delta_g$	1	1	0	2.210
VCl_2	$^4\Sigma_g^-$	2	1	0	2.164
$CrCl_2$	$^5\Pi_g$	2	1	1	2.130
$MnCl_2$	$^6\Sigma_g^+$	2	1	2	2.147
$FeCl_2$	$^5\Delta_g$	3	1	2	2.141
$CoCl_2$	$^4\Sigma_g^-$	4	1	2	2.103
$NiCl_2$	$^3\Sigma_g^-$	4	2	2	2.060
$CuCl_2$	$^2\Pi_g$	4	2	3	2.047
$ZnCl_2$	$^1\Sigma_g^+$	4	2	4	2.078

$^4\Delta_g \longleftarrow {}^4\Sigma_g^-$, the band at 9600 cm^{-1} as $^4\varphi_g \longleftarrow {}^4\Sigma_g^-$ and the band at 10700 cm^{-1} as $^4\Pi_g \longleftarrow {}^4\Sigma_g^-$.

Table 8 lists the calculated ground terms, strong-field configurations and bond lengths for the 3d transition metal dichlorides (including $CaCl_2$ and $ZnCl_2$) obtained using the BP86 functional and all electron triple-ζ basis sets with the DeFT code. Fig. 10 shows the variation in the bond lengths and the bond orders for these systems. All of the molecules are predicted to be linear. As the metal is at the centre of the molecule, it is possible to fully decompose the bond order into the contributions from the orbitals of σ_g, σ_u, π_g, π_u and δ_g symmetry and this is shown in Fig. 10(b).

The overall trend is for the bond lengths to decrease across the series as expected. The dotted line in Fig. 10(a) connects the bond lengths in $CaCl_2$, $MnCl_2$ and $ZnCl_2$ which each contain a spherically occupied d-shell (d^0, d^5 and d^{10} respectively). The deviations from this line are of the 'double-hump' form familiar in the solid-state dihalides. Fig. 8 shows the CFSE for a linear and octahedral complex calculated using the crystal-field d-orbital energies. The variation in the CFSE for the octahedral complex shows the expected double-hump with maxima at d^3 and d^8 corresponding to filling of the t_{2g} shell. The variation in the CFSE for the linear molecules is predicted to be a little more complex with maxima at d^2 and d^7 and sharp changes in the gradient at d^4 and d^9. The bond lengths, however, show little evidence for such variation and indeed more closely resemble the octahedral case. This is a direct result of the failure of crystal-field theory to predict the correct d-orbital ordering. As described above, the effect of d–s mixing is to make the d_σ orbital approximately non-bonding in character. There are thus three non-bonding d-orbitals (two of δ_g symmetry and one of σ_g symmetry) and two strongly antibonding d-orbitals (of π_g symmetry). In octahedral complexes, there are also three approximately non-bonding d-orbitals (of t_{2g} symmetry and of π type) and two strongly antibonding d-orbitals (of e_g symmetry and of σ type). The true d-electron stabilization energies vary in a very similar manner for the two symmetries. Similar behaviour has also been noted in the bond length variations of the monoxide and monosulfide molecules.[5a]

Fig. 10(b) shows that there is an overall increase in the M–Cl bond order across the transition metal series mirroring the overall contraction in bond lengths. However, the variation between the elements is more complicated as revealed by the breakdown into symmetry types. The σ_u and π_u contributions both show gradual growth both in absolute and relative terms across the series. This reflects both the increased $Cl^- \rightarrow M^{2+}$ donation associated with the higher metal electropositivity and the greater importance of the metal p-orbitals to the bonding. The analysis shows that the p-orbitals contribute *ca.* 25% to the bond order in $CaCl_2$ and *ca.* 50% to the bond order in $ZnCl_2$.

The variation in the π_g contribution displays a more pronounced sensitivity to the d^n configuration. Between d^0 and d^3, the π_g contribution increases as the M–Cl bond length decreases. Between d^4 and d^5, however, electrons are added to the antibonding $2\pi_g$ orbitals causing a large drop in the π_g contribution and an increase in the bond length. This is mirrored in the second half of the d-block but the decreased radial extension of the d-orbitals greatly reduces their role in the bonding and the changes are much smaller. In $ZnCl_2$, the π_g contribution is minor as the radial contraction leads to effectively core-like d-orbitals. The σ_g contribution is approximately constant from $CaCl_2$ to $CuCl_2$ reflecting the non-bonding character of the $s–d_\sigma$ hybrid. The core-like nature of the d-orbitals in $ZnCl_2$ leads to σ-bonding being entirely due to the zinc 4s leading to an increase in the contribution. The analysis thus shows that the π contribution is predicted to be *larger* than the σ-contribution for $ScCl_2$ (d^1)–$CrCl_2$ (d^4).

Conclusions

The utility of the Mayer bond order has been tested in a number of inorganic molecules ranging from simple main group molecules such as diatomics and classical octet systems, molecules containing multicentre and delocalized interactions, hypervalent systems and transition metal complexes. The decomposition of the bond order into contributions from symmetry types has been demonstrated and its usefulness in the description of bonding within LCAO theory has been examined. The basis set dependence of the Mayer bond order has been investigated and the nature of the bond order/bond length correlation has been examined for a number of different bond types.

The Mayer bond order has a similar basis set dependence as the Mulliken charge to which it is closely related. Thus, it is not possible to predict absolute values within a finite basis and comparison between different systems is only valid if identical or analogous basis sets are used. The dependence of the bond order, and by extension the dependence of other bonding analysis tools such as Mulliken charges, NBO charges, AIM charges, bond ellipticities and bond orders, on the density functional method is found to be small. Differences in the character of the orbitals produced by local, non-local and hybrid DFT methods arise primarily from the different geometries produced rather than fundamental differences in the density matrices.

For many interactions of interest to inorganic chemists, such as the metal–ligand bonds in mononuclear complexes, it has been shown that the Mayer bond order is simply a sum of the bond orders for each symmetry type involved. In other molecules, the bond order can often be decomposed into σ and π contributions. Such an analysis allows deeper insight into the nature of the bonding and how it varies with, for example, the d^n configuration in transition metal complexes and the ring size in S–N rings.

In this paper, we have attempted to show how the Mayer bond order allows the results of high-level computational studies to be understood in terms of the LCAO and symmetry adapted models that form the underlying language in which most inorganic chemists describe molecular structure. Although the role and usefulness of symmetry theory has been at the forefront of this work, it is worth noting that probably the main advantage in using the Mayer bond order arises in large compounds with little or no symmetry. In such systems, the bonding between two atomic centres arises from very many orbitals. Many of these orbitals will give rise to bond interactions and some will lead to antibonding orbitals. Without the advantage of symmetry, it can be very difficult to describe the sum of these interactions and the computational chemist often restricts the analysis to the high-lying occupied orbitals and the low-lying virtual orbitals. The Mayer bond order provides a convenient and computationally efficient method of summing *all* of the contributions to the bond. This has been shown in a number of our previous studies including an analysis of the bonding in the ground state of a tetragonally compressed copper(II) complex[48] and in a comparison of sandwich complexes of arene and B–N rings.[4c] Although the geometries of these systems approximate to higher symmetry structures, it is not necessary to build in this approximation to analyse the bonding when the bond order is used and, indeed, the role of the small distortions can be examined.

Acknowledgements

The authors would like to thank the EPSRC, the Cambridge Overseas Trust, Selwyn College (Cambridge) and the University of Hull for financial support, and the Computational Chemistry Working Party for access to the computational facilities in the Rutherford-Appleton Laboratory.

References

1 C. A. Coulson, *Proc. R. Soc. London*, *Ser. A*, 1939, **169**, 413; C. A. Coulson, *Proc. R. Soc. London*, *Ser. A*, 1951, **207**, 91; C. A. Coulson, *Valence*, 2nd edn., Oxford University Press, London, 1961.
2 K. A. Wiberg, *Tetrahedron*, 1968, **24**, 1083.
3 I. Mayer, *Chem. Phys. Lett.*, 1983, **97**, 270; I. Mayer, *Int. J. Quantum Chem.*, 1984, **26**, 151.
4 (*a*) A. J. Bridgeman, N. Harris and N. A. Young, *Chem. Commun.*, 2000, 1241; (*b*) A. J. Bridgeman and N. A. Nielsen, *Inorg. Chim. Acta*, 2000, **303**, 107; (*c*) A. J. Bridgeman and J. Rothery, *J. Chem. Soc.*, *Dalton Trans.*, 1999, 4077; (*d*) A. J. Bridgeman and J. Rothery, *Inorg. Chim. Acta*, 1999, **288**, 17; (*e*) A. J. Bridgeman, *Polyhedron*, 1998, **17**, 2279; (*f*) A. J. Bridgeman, *J. Chem. Soc.*, *Dalton Trans.*, 1997, 2887; (*g*) A. J. Bridgeman, *J. Chem. Soc.*, *Dalton Trans.*, 1997, 1323.
5 (*a*) A. J. Bridgeman and J. Rothery, *J. Chem. Soc.*, *Dalton Trans.*, 2000, 211; (*b*) A. J. Bridgeman, *J. Chem. Soc.*, *Dalton Trans.*, 1996, 2601; (*c*) A. J. Bridgeman, *J. Chem. Soc.*, *Dalton Trans.*, 1997, 4765; (*d*) A. J. Bridgeman and C. H. Bridgeman, *Chem. Phys. Lett.*, 1997, **272**, 173.
6 L. Pauling, L. O. Brockway and H. Y. Beach, *J. Am. Chem. Soc.*, 1935, **57**, 2705; L. Pauling, *J. Am. Chem. Soc.*, 1947, **69**, 542; L. Pauling, *The Nature of the Chemical Bond*, Cornell University Press, New York, 1960.
7 G. Lendvay, *THEOCHEM*, 2000, **501**, 389.
8 M. J. Frisch, G. W. Trucks, H. B. Schlegel, G. E. Scuseria, M. A. Robb, J. R. Cheeseman, V. G. Zakrzewski, J. A. Montgomery, Jr., R. E. Stratmann, J. C. Burant, S. Dapprich, J. M. Millam, A. D. Daniels, K. N. Kudin, M. C. Strain, O. Farkas, J. Tomasi, V. Barone, M. Cossi, R. Cammi, B. Mennucci, C. Pomelli, C. Adamo, S. Clifford, J. Ochterski, G. A. Petersson, P. Y. Ayala, Q. Cui, K. Morokuma, D. K. Malick, A. D. Rabuck, K. Raghavachari, J. B. Foresman, J. Cioslowski, J. V. Ortiz, B. B. Stefanov, G. Liu, A. Liashenko, P. Piskorz, I. Komaromi, R. Gomperts, R. L. Martin, D. J. Fox, T. Keith, M. A. Al-Laham, C. Y. Peng, A. Nanayakkara, C. Gonzalez, M. Challacombe, P. M. W. Gill, B. Johnson, W. Chen, M. W. Wong, J. L. Andres, C. Gonzalez, M. Head-Gordon, E. S. Replogle and J. A. Pople, Gaussian 98, Revision A.3, Gaussian, Inc., Pittsburgh, PA, 1998.
9 M. Dupuis, D. Spangler and J. Wendoloski, NRCC Software Catalog, vol. 1, program no. QG01 (GAMESS), University of California, Berkeley, CA, 1980; M. F. Guest, J. Kendrick, J. H. Van Lenthe, K. Shoeffel and P. Sherwood, *GAMESS-UK Users Guide and Reference Manual*, version 5, Computing for Science (CFS) Ltd., Daresbury Laboratory, 1994.
10 E. J. Baerends, D. E. Ellis and P. Ros, *Chem. Phys.*, 1973, **2**, 41; L. Versluis and T. Ziegler, *J. Chem. Phys.*, 1988, **322**, 88; G. te Velde and E. J. Baerends, *J. Comput. Phys.*, 1992, **99**, 84; C. Fonseca Guerra, J. G. Snijders, G. te Velde and E. J. Baerends, *Theor. Chem. Acc.*, 1998, **99**, 391.
11 A. St-Amant, DeFT, University of Ottawa, 1994.
12 S. H. Vosko, L. Wilk and M. Nusair, *Can. J. Phys.*, 1980, **58**, 1200.
13 A. D. Becke, *Phys. Rev. A*, 1988, **38**, 3098.
14 J. P. Perdew, *Phys. Rev. B*, 1986, **33**, 8822.
15 C. Lee, W. Yang and R. G. Parr, *Phys. Rev. B*, 1988, **37**, 785.
16 A. D. Becke, *J. Chem. Phys.*, 1993, **98**, 5648.
17 E. D. Glendening, A. E. Reed, J. E. Carpenter and F. Weinhold, NBO version 3.1, University of Wisconsin, WI, 1995.
18 R. F. W. Bader, *Atoms in Molecules: a Quantum Theory*, Oxford University Press, Oxford, 1990.
19 J. Cioslowski and S. T. Mixon, *J. Am. Chem. Soc.*, 1991, **113**, 4142.
20 A. J. Bridgeman, MAYER, University of Hull, 2001. (Available on request from the authors.)
21 For example; P. W. Atkins, *Physical Chemistry*, 6th edn., Oxford University Press, Oxford, 1998; C. E. Housecroft and A. G. Sharpe, *Inorganic Chemistry*, Prentice-Hall, Harlow, 2001.
22 S. S. Shaik A. Shurki, D. Danovich and P. C. Hiberty, *THEOCHEM*, 1997, **398**, 155; P. C. Hibery, D. Danovich, A. Shurki and S. Shaik, *J. Am. Chem. Soc.*, 1995, **117**, 7760; P. C. Hibery, G. Ohanessian, S. S. Shaik and J. P. Flament, *Pure Appl. Chem.*, 1993, **65**, 35.
23 M. L. deLucia and P. Coppins, *Inorg. Chem.*, 1978, **17**, 2336.
24 A. E. Reed, R. B. Weinstock and F. Weinhold, *J. Chem. Phys.*, 1985, **83**, 735.
25 A. G. MacDiarmid, C. M. Mikulski, P. J. Russo, M. S. Saran, A. F. Garito and A. J. Heeger, *J. Chem. Soc.*, *Chem. Commun.*, 1975, 476; A. J. Banister, H. G. Clarke, I. Rayment and H. M. M. Shearer, *Inorg. Nucl. Chem. Lett.*, 1974, **10**, 647; J. Bojes, T. Chivers, W. G. Laidlaw and M. Trsic, *J. Am. Chem. Soc.*, 1979, **101**, 4517; H. W. Roesky, *Adv. Inorg. Chem. Radiochem.*, 1979, **22**, 239; R. J. Gillespie, D. R. Slim and J. D. Tyrer, *J. Chem. Soc.*, *Chem. Commun.*, 1977, 253; A. C. Hazell and R. G. Hazell, *Acta Chim. Scand.*, 1972, **26**, 1987.
26 P. Popelier, *Atoms in Molecules*, Pearson Education, Harlow, 2000.
27 L. T. Molina and M. J. Molina, *J. Phys. Chem.*, 1987, **91**, 433.
28 M. Birk, R. R. Friedl, E. A. Cohen, H. M. Pickett and S. P. Sander, *J. Chem. Phys.*, 1989, **91**, 6588.
29 M. P. McGrath, K. C. Clemitshaw, F. S. Rowland and W. J. Hehre, *J. Phys. Chem.*, 1990, **94**, 6126; F. Jensen and J. Oddershede, *J. Phys. Chem.*, 1990, **94**, 2235; J. B. Burkholder, J. J. Orlando and C. J. Howard, *J. Phys. Chem.*, 1990, **94**, 687; M. J. Molina, A. J. Colussi, L. T. Molina, R. N. Schindler and T. L. Tso, *Chem. Phys. Lett.*, 1990, **173**, 310; I. J. Eberstein, *J. Geophys. Res. Lett.*, 1990, **17**, 721; W. B. DeMore and E. Tschuikow-Roux, *J. Phys. Chem.*, 1990, **94**, 5556; S. Abramowitz and M. W. Chase, Jr., *Pure Appl. Chem.*, 1991, **63**, 1449; J. Jacobs, M. Kronberg, H. S. P. Müller and H. Willner, *J. Am. Chem. Soc.*, 1994, **116**, 1106; K. J. Huder and W. B. DeMore, *J. Phys. Chem.*, 1995, **99**, 3905; M. Schwell, H.-W. Jochims, B. Wassermann, U. Rockland, R. Flesch and E. Rühl, *J. Phys. Chem.*, 1996, **100**, 10070; W.-K. Li and C.-Y. Ng, *J. Phys. Chem.*, 1997, **101**, 113.
30 M. A. Clyde and J. A. Coxon, *Proc. R. Soc. London*, *Ser. A*, 1968, **303**, 207; N. Basco and S. K. Dogra, *Proc. R. Soc. London*, *Ser. A*, 1971, **333**, 41; M. A. Clyde and R. T. Watson, *J. Chem. Soc.*, *Faraday Trans.*, 1975, **71**, 336; S. P. Sander and R. T. Watson, *J. Phys. Chem.*, 1981, **85**, 2960.
31 Y. L. Yung, J. P. Pinto, R. T. Watson and S. P. Sander, *J. Atmos. Sci.*, 1980, **37**, 339.
32 D. W. Toohey and J. G. Anderson, *J. Phys. Chem.*, 1988, **92**, 1705.
33 J. S. Francisco, S. P. Sander, T. J. Lee and A. P. Rendell, *J. Phys. Chem.*, 1994, **98**, 5644.

34 T. J. Lee, C. M. Rohlfing and J. E. Rice, *J. Chem. Phys.*, 1992, **97**, 6593; D. Christen, H.-G. Mack and H. S. P. Müller, *THEOCHEM*, 1999, **137**, 509.
35 J. T. Gleghorn, *Chem. Phys. Lett.*, 1997, **271**, 296.
36 S. Guha and J. S. Francisco, *J. Phys. Chem. A*, 1996, **101**, 5347.
37 D. Papayannis, A. M. Kosmas and V. S. Melissas, *Chem. Phys.*, 1999, **243**, 249.
38 P. Marshall and A. Misra, *J. Chem. Soc.*, *Faraday Trans.*, 1997, **93**, 3301.
39 P. Marshall and A. Misra, *J. Phys. Chem. A*, 1998, **102**, 9056.
40 M. Hargittai, *Chem. Rev.*, 2000, **100**, 2233.
41 D. W. Smith, *Inorg. Chim. Acta*, 1971, **5**, 231.
42 S. H. Ashworth, F. J. Grieman and J. M. Brown, *Chem. Phys. Lett.*, 1990, **175**, 660; S. H. Ashworth, F. J. Grieman, J. M. Brown, P. J. Jones and I. R. Beattie, *J. Am. Chem. Soc.*, 1993, **115**, 2978.
43 T. Tokuda, N. Fujii, S. Yoshuda, K. Shimuza and I. Tanaka, *Chem. Phys. Lett.*, 1990, **174**, 385; A. J. Bouvier, R. Bacis, J. Bonnet, S. Churassy, P. Crozet, B. Erba, J. B. Koffend, J. Lamarre, D. Pigache and A. J. Ross, *Chem. Phys. Lett.*, 1991, **184**, 133; H. P. Yang, Y. Qin, Q. N. Yuan, X. B. Xie, Q. Zhuang and C. H. Zhuang, *Chem. Phys. Lett.*, 1992, **191**, 130; T. Tokuda and N. Fujii, *J. Phys. Chem.*, 1992, **96**, 6504; P. Crozet, A. J. Ross, R. Bacis, M. P. Barnes and J. M. Barnes, *J. Mol. Spectrosc.*, 1995, **43**, 172; A. J. Ross, R. Bacis, A. J. Bouvier, S. Churassy, J.-C. Coste, P. Crozet and I. Russier, *J. Mol. Spectrosc.*, 1995, **158**, 27.
44 C. W. Bauschlicher, Jr. and B. O. Roos, *J. Chem. Phys.*, 1989, **91**, 4785; R. J. Deeth, *J. Chem. Soc.*, *Dalton Trans.*, 1993, 1061; F. Rogemond, H. Chermette and D. R. Salahub, *Chem. Phys. Lett.*, 1994, **219**, 228.
45 A. J. Bridgeman and M. Gerloch, *Prog. Inorg. Chem.*, 1997, **45**, 179.
46 C. E. Schaffer, *Inorg. Chim. Acta*, 1995, **240**, 581.
47 C. W. DeKock and D. M. Gruen, *J. Chem. Phys.*, 1966, **44**, 4387.
48 A. J. Bridgeman, M. A. Halcrow, M. Jones, E. Krausz and N. K. Solanki, *Chem. Phys. Lett.*, 1999, **314**, 176.